Tunable light-drag effects in Cu_2O

M. Artoni,[1] G. C. La Rocca,[2,3] I. Carusotto,[4,2] and F. Bassani[2]
[1]*INFM, European Laboratory for Non-linear Spectroscopy, Largo E. Fermi 2, Florence, Italy*
[2]*INFM, Scuola Normale Superiore, Piazza dei Cavalieri 7, 56126 Pisa, Italy*
[3]*Dipartimento di Fisica, "E. R. Caianiello," Università di Salerno, 84081 Baronissi (Sa), Italy*
[4]*Laboratoire Kastler-Brossel, Ecole Normale Superieure, 24 rue Lhomond, 75231 Paris Cedex 05, France*
(Received 13 April 2001; revised manuscript received 8 November 2001; published 6 June 2002)

We develop a general theory of the Fresnel light drag for nonstationary boundaries and one in which frequency and angular dispersion of the dragging medium are both included. We apply the theory to investigate a Fizeau-type optical interferometer that uses coherently driven cuprous oxide (Cu_2O) as dragging medium. For such a material, where electromagnetically induced transparency can be implemented through a typical pump-probe configuration, the resonant probe-beam experiences a phase shift (Fresnel-Fizeau effect) that may vary over a wide range of values, positive or negative, or it may even vanish due to the combined effects of the strong frequency dispersion and anisotropy both induced by the pump. Our drag values are compared with those obtained by using standard dragging materials as well as with those where neutron rather than light waves are being dragged. The similarities between matter and light waves yield essential insights into the nature of the dragging effect with massive and massless particles.

DOI: 10.1103/PhysRevB.65.235422 PACS number(s): 03.30.+p, 42.50.Gy

I. INTRODUCTION

The phase velocity of light depends on whether light propagates in a moving or in a stationary medium. This effect, which gives rise to the familiar Fresnel light drag,[1,2] was observed for the first time in Fizeau's flowing water experiment[3] and had a profound influence on the change of our perception[2] of the nature of space and time at the turn of the century. Fizeau's confirmation of the Fresnel light drag was at first considered one of the greatest triumph of ether theory. However, the fact that the Fresnel-drag effect was indeed contained[4] in the special theory of relativity along with the Michelson-Morley experiment establishing the constancy of the speed of light in vacuum[5] opened the way to a different interpretation of the drag effect, namely one in terms of different inertial observer's views of events, which then became a resting foundation over which the theory of relativity was built.

Light-drag experiments have been repeated more accurately in the intervening years, in particular, by Michelson-Morley in flowing water[6] and quite extensively by Zeeman in quartz[7] and flint glass.[8] The higher level of accuracy required the inclusion of dispersive terms which were just ignored by Fresnel's 1818 theory and which are due to the wavelength dependence of the dragging medium refractive index. The advent of ring lasers spurred further high-precision measurements of light drags[9] because the measurable quantity was a beat frequency rather than a phase shift between counter-propagating beams. Bilger, Zavodny and Stowell,[10] e.g., placed a rotating fused silica disk[11] into an arm of a ring laser with light entering at oblique incidence off center the plane face of the disk while subsequently Sanders and Ezeckiel[12] achieved an even better accuracy by shuttling glass samples to and fro along the beam path of a passive ring resonator.

Although different dragging media and diverse interferometric measurement techniques have been employed to carry out increasingly precise measurements of light drags,[6,12] these have not reached the level of precision of other tests of special relativity.[12] In order to perform a high-precision measurement of the Fresnel-Fizeau effect one needs high sensitivity to velocity-induced phase shifts which sets a lower bound for the usable sample speeds. At the same time, in order to preserve high contrast of the interference fringe pattern, mechanical vibrations from the sample movement have to be otherwise minimized. We here anticipate that this goal can be achieved by using as a dragging medium a slab of cuprous oxide (Cu_2O) that exhibits electromagnetically induced transparency[13] (EIT): interferometric sensitivity at low drag velocities can be increased by at least one order of magnitude.

Higher levels of measurement precision should require, on the other hand, a higher level of accuracy in the derivation of the expected drag coefficient to include for corrections that are otherwise commonly neglected. Small tilt angles (θ_0) are required, e.g., to avoid multiple internal reflections and to minimize the effect of backreflections of light into the interferometer beam path[12] yet without causing strong deflections of the beam off the optical axis of the arm interferometer (see Fig. 1). This complicates considerably the derivation of the theoretical light-drag value to be compared with the experimental one. Refraction at the inclined boundaries gives rise, in fact, to geometrical path changes, i.e., a misalignment (φ_I) between the beam path and the optical axis of the interferometer arm as well as aberration effects which stem from changes between the sample rest frame and the laboratory frame. These should be taken in the proper account in order to minimize the discrepancy between theory and experiment.

Furthermore, in a Cu_2O sample that is coherently driven by a pump and probe beam in a typical Λ configuration,[13] a suitable choice of the pump and probe polarizations can also make the light drag vanish for all velocities of experimental interest and over a broad range of optical frequencies simply by varying the pump parameters. This means that in a typical

 ©2002 The American Physical Society

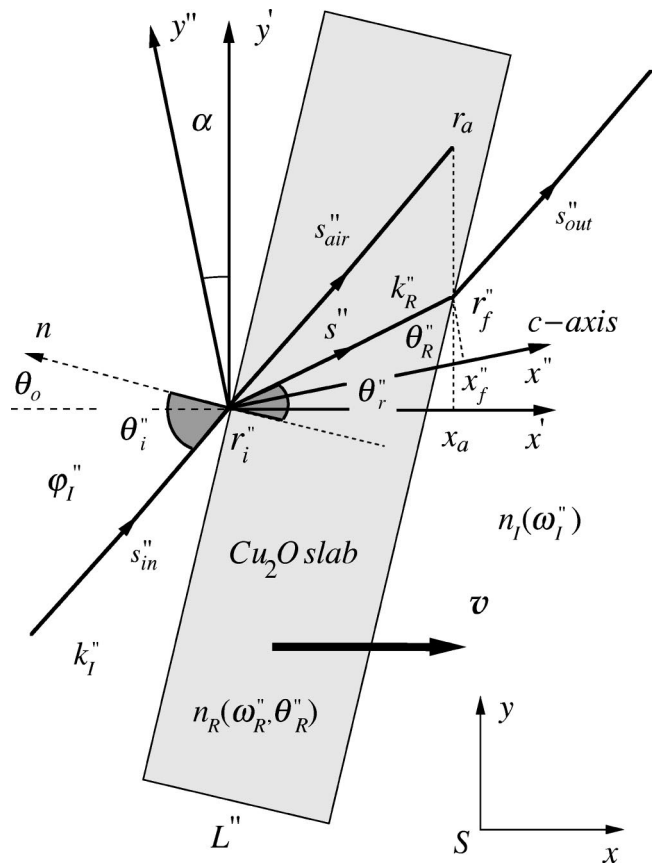

FIG. 1. Path taken by a beam propagating through a moving Cu_2O slab along the arm of an interferometer used for a high-precision measurement of the Fresnel drag coefficient. The axis of the interferometer arm is parallel to the x axis. The slab induces the light drag (32) as it moves with respect to an observer in the laboratory frame S and with constant velocity v directed in the positive x direction. The beam wave vector makes an angle φ_I'' (outside) and $\varphi_R''=\theta_R''+\alpha$ (inside) with respect to $\boldsymbol{v}$. The beam direction with respect to the medium optical c axis (x''), kept fixed at an angle α with respect to x, is determined by θ_R''. The slab tilt angle (θ_0) with respect to the x axis and the incident (θ_i'') and refracted (θ_r'') angles satisfy the relation $\theta_i''-\varphi_I''=\theta_r''-\varphi_R''=\theta_0$. All angles are given here as seen in the slab rest frame S''.

interferometric experiment no fringe shift would be observed for light propagating through a moving medium with respect to light propagating through the same medium at rest. Such a somewhat surprising conclusion has been so far found to hold only in the very different context of neutron de Broglie waves in moving matter.[39]

The aim of the present paper is thus twofold. First, we improve theoretical predictions of the drag by including[14] appreciable corrections associated with light beam refraction inside a moving sample that commonly are not fully accounted for. Second, we devise a scheme that employs electromagnetically induced transparency to tune the drag magnitude over a very interesting range of values. Depending on the external pump parameters, the use of such a scheme enables one to readily span the drag from vanishing values up to unusually large ones.

We provide in Sec. II a detailed derivation of the light-drag coefficient of a slab slowly moving through a medium having a different refractive index. This is done by adopting a first-principles formalism which takes into account the combined effects of frequency dispersion and anisotropy. In this and in the following Sec. III we provide closed-form expressions for two common forms of drag, i.e., the effective[12] and absolute[15] drag coefficients. In Sec. IV we examine how suitable choices of the pump and probe polarizations can render a sample of cuprous oxide (Cu_2O) under EIT uniaxial[16] and transparent. We then use the general theory for light drags in a uniaxial medium developed in Sec. II to demonstrate that using cuprous oxide under EIT as dragging medium may enable one to make the drag to change sign or even vanish over a broad range of optical frequencies. The discussion of how this may improve the level of accuracy of optical drag experiments is done in Sec. V. The main results along with a thorough comparison with drag experiments using matter rather than light waves are finally discussed in Sec. VI while detailed calculations needed to derive the general results of Secs. II and III are reported in the three Appendixes.

II. PHASE SHIFT AND EFFECTIVE DRAG COEFFICIENT

The dragging medium, in the form of a parallel-sided slab that is commonly placed in one arm of a high-precision interferometer,[9,12] induces an optical phase shift which we here calculate from first principles including the effects of frequency and angular dispersion. The phase shift is in general associated with a space–time contour, i.e., $\Delta\phi=\oint(\omega\,dt-\boldsymbol{k}\cdot d\mathbf{r})$, which accounts for the temporal and spatial changes that a plane-wave of wave vector $\boldsymbol{k}$ and angular frequency ω undergoes as it propagates through the medium. In our approach we set all times to be identical and we evaluate $\oint\boldsymbol{k}\cdot d\mathbf{r}$ across the interferometer arm length. Phase shifts depend crucially on boundary conditions. Unlike in the historic work of Fizeau,[3] where the phase shifts were produced by water flowing inside stationary tubes, we will consider here a configuration in which the medium boundaries are in motion. The relevant geometry is illustrated in Fig. 1 where the slab is shown to move along the interferometer arm with constant[17] velocity v with respect to an observer in the laboratory frame S. Its velocity is directed in the positive x direction of S which also defines the (optical) axis of the interferometer arm. The sample is tilted (θ_0) with respect to this axis while the beam impinges off the surface normal (θ_i) and is subsequently refracted (θ_r) through the medium[18]. The tilt causes a misalignement (φ_I), i.e., a deflection of the beam path off the axis.

The sample rest frames S' and S'' are rotated with respect to one another by a fixed angle α about the z axis and the coordinate axis x' is oriented in the direction of v. The space-time coordinates as well as the frequency and wave vector of the light wave in S and S'' are connected through a Lorentz transformation[15] which comprises a boost from S to S' and a rotation about the z axis from S' to S'',

$$t''=\gamma\left(t-\beta\frac{x}{c}\right),\quad \omega''=\gamma(\omega-vk_x),$$

$$x''=\gamma(x-vt)\cos\alpha+y\sin\alpha,$$

$$k_x''=\gamma\left(k_x-\beta\frac{\omega}{c}\right)\cos\alpha+k_y\sin\alpha,$$

$$y''=-\gamma(x-vt)\sin\alpha+y\cos\alpha,$$

$$k_y''=-\gamma\left(k_x-\beta\frac{\omega}{c}\right)\sin\alpha+k_y\cos\alpha,$$

$$z''=z,\quad k_z''=k_z, \tag{1}$$

where $\beta=v/c$ and $\gamma=(1-\beta^2)^{-1/2}$. Because the phase shift is relativistically invariant under the combined transformation (1), that is,

$$\Delta\phi=(k^\mu\Delta x_\mu)|_{\Delta t=0}=(k''^\mu\ \Delta x''_\mu)|_{\Delta t=0}, \tag{2}$$

we find it convenient to derive its expression first in the slab rest frame S''. We adopt the compact four-vector notation $k^\mu=(\omega/c,\boldsymbol{k})$ and $x_\mu=(ct,-\boldsymbol{r})$ and a similar one for k''^μ and x''_μ. To the lowest order in β, the *single-pass* phase shift of the beam traversing the sample clockwise for the specific configuration of Fig. 1 is

$$\Delta\phi\simeq-k_R''s''-\beta\frac{\omega_R''}{c}(x_f-x_i)|_{\Delta t=0}$$
$$=-\frac{\omega_R''L''}{c}\left\{\frac{\mathrm{Re}[n_R(\omega_R'',\theta_R'')]+\beta\cos(\theta_r''-\theta_0)}{\cos\theta_r''}\right\}, \tag{3}$$

where L'' is the actual thickness of the slab, s'' is the beam-path length through the moving sample, and k_R'' is the real part of the beam wave vector. In the last expression on the right-hand side of Eq. (3) we used the fact that

$$x_f-x_i=s''\cos\varphi_R''=s''\cos(\theta_r''-\theta_0), \tag{4}$$

when $\Delta t=t_f-t_i=0$, while $n_R(\omega_R'',\theta_R'')$ is the sample rest frame complex refractive index which accounts in general for both frequency and angular dispersion.

We proceed to write the shift $\Delta\phi$ in terms of the laboratory frame angles and frequencies. We specialize our analysis to the shift experienced by a plane *extraordinary* wave in a generic *uniaxial* medium.[16] In this case θ_R'' on the right-hand side of Eq. (3) denotes the angle between the refracted beam wave vector and the optical c axis. Because our medium is homogeneous but not isotropic, the group velocity and phase velocity of the light wave propagating through the medium will not be parallel when viewed in S''; i.e., ray vectors and wave vectors do not coincide[16] in the sample rest frame. For the specific situation that we examine in the following, this, however, turns out to be immaterial and we can take the beam path $\boldsymbol{s}''$ parallel[19] to the beam wave vector.[20]

Because the slab surfaces are stationary in S'', there is no frequency change at the sample boundaries, i.e., $\omega_R''=\omega_I''$ and hence $n_R(\omega_R'',\theta_R'')=n_R(\omega_I'',\theta_R'')$. We distinguish between refracted angles and frequencies, defined inside the medium, and the corresponding incident ones, defined outside the medium, by using the two distinct suffixes R and I. Doppler shifts and aberrations are quite little for very small slab velocities and the refractive index can then be expanded as[21]

$$n_R(\omega_R'',\theta_R'')\simeq n_R^0(\omega_I,\theta_R)+\frac{\partial n_R(\omega_I'',\theta_R'')}{\partial\omega_I''}(\omega_I''-\omega_I)$$
$$+\frac{\partial n_R(\omega_I'',\theta_R'')}{\partial\theta_R''}(\theta_R''-\theta_R), \tag{5}$$

where $n_R^0(\omega_I,\theta_R)$ is the lowest-order contribution to the laboratory frame refractive index of the sample and where the derivatives are to be evaluated respectively at $\omega_I''=\omega_I$ and $\theta_R''=\theta_R$. A boost to the lowest order in β from S to S'' yields, for the Doppler shift (first-order Doppler),

$$\omega_I''\simeq\omega_I-\beta\omega_I\mathrm{Re}[n_I(\omega_I)]\cos\varphi_I, \tag{6}$$

where $n_I(\omega_I)$ is the laboratory frame refractive index of the medium outside the slab, while for the aberration inside the slab,

$$\varphi_R''\simeq\varphi_R+\beta\omega_R\frac{\sin\varphi_R}{k_Rc}=\varphi_R+\frac{\beta\sin\varphi_R}{\mathrm{Re}[n_R(\omega_R,\theta_R)]}, \tag{7}$$

where the real parts arise from the fact that the Lorentz transformation (1) is defined for real wave vector components. The second form of Eq. (7) specifically applies to a plane *extraordinary* wave. A similar expression holds for φ_I'' in the isotropic medium outside the slab upon the interchange $R\to I$.

Here φ_R'' (φ_I'') is the angle between the refracted (incident) beam and the slab velocity direction. Since $\varphi_R''=\theta_R''+\alpha$ and likewise $\varphi_R=\theta_R+\alpha$, it follows that

$$\theta_R''\simeq\theta_R+\frac{\beta\sin\varphi_R}{\mathrm{Re}[n_R(\omega_R,\theta_R)]}\simeq\theta_R+\frac{\beta\sin\varphi_R}{\mathrm{Re}[n_R^0(\omega_I,\theta_R)]}. \tag{8}$$

We used the transformation law of the phase velocity in an infinite medium to replace $n_R(\omega_R,\theta_R)$ in Eq. (8) by the lowest-order refractive index contribution $n_R^0(\omega_I,\theta_R)$ as discussed in detail in Appendix A. When Eqs. (6) and (8) are substituted in to Eq. (5) and its real part is in turn substituted back into Eq. (3) along with Eqs. (6) and (7), we obtain, for the phase shift,

$$\Delta\phi=-\frac{\omega_IL''}{c}\frac{\mathrm{Re}[n_R^0]}{\cos\theta_r}-\beta\frac{\omega_IL''}{c}\frac{\sin\varphi_R}{\cos\theta_r}\left(\tan\theta_r+\frac{\mathrm{Re}[\mathcal{D}_\theta]}{\mathrm{Re}[n_R^0]}\right)$$
$$-\beta\frac{\omega_IL''}{c}\frac{\cos\varphi_R}{\cos\theta_r}\left[1-\frac{\cos\varphi_I}{\cos\varphi_R}\mathrm{Re}[n_I](\mathrm{Re}[n_R^0]\right.$$
$$\left.+\omega_I\mathrm{Re}[\mathcal{D}_\omega])\right]\equiv\Delta\phi_0-\beta\frac{\omega_IL''}{c}\alpha_e, \tag{9}$$

where higher-order terms in the slab velocity are omitted. Unless otherwise stated, the following shorthand notation for the first and second derivative terms on the right-hand side of Eq. (5),

$$\mathcal{D}_\omega \to \left.\frac{\partial n_R(\omega_I'',\theta_R'')}{\partial \omega_I''}\right|_{\substack{\omega_I''=\omega_I\\ \theta_R''=\theta_R,}}$$

$$\mathcal{D}_\theta \to \left.\frac{\partial n_R(\omega_I'',\theta_R'')}{\partial \theta_R''}\right|_{\substack{\omega_I''=\omega_I\\ \theta_R''=\theta_R,}} \tag{10}$$

and

$$n_I \to n_I(\omega_I), \quad n_R^0 \to n_R^0(\omega_I,\theta_R), \tag{11}$$

will be hereafter adopted.

In the specific case in which the slab moves in vacuum ($n_I=1$) and with velocity $\boldsymbol{v}$ parallel to the surface normal ($\theta_0=0$) and to the incident light beam ($\varphi_I=\varphi_R=0$), then α_e in Eq. (9) recovers exactly the effective drag coefficient discussed by Sanders and Ezekiels in Refs. 12 and 22. Note, however, that in the case of a tilted slab ($\theta_0\neq 0$) moving through a surrounding medium of real refractive index n_I and no misalignement is accounted for ($\varphi_I=0$) we find a slightly different form of the effective drag α_e because aberration effects have apparently been neglected in Ref. 12.

The single-pass shift $\Delta\phi$ in Eq. (9) gives the relative phase of the incident and emerging light beams as viewed from the laboratory frame S when Doppler frequency shifts, effects of refraction at the inclined boundaries of the slab, and angular dispersion of the medium are accounted for. Here $\Delta\phi_0$ denotes the familiar shift induced by a stationary sample while the additional term on the right-hand side of Eq. (9) stems from the slab motion and defines in turn the light-drag coefficient α_e. The first of the two contributions to the drag comprises a term arising from the medium angular dispersion and another one arising from the velocity dependence of the refracted beam-path through the sample. The latter is directly related, as discussed in detail in Appendix B, to the aberration suffered by both incident and refracted beams when boosted from S to S''. The next contribution to the drag on the right-hand side of Eq. (9) is what is most commonly observed in Fresnel light-drag experiments.[12] Aberration is relevant to this term as well but only indirectly, i.e., through the appropriate value for the refracted angle θ_r, or θ_R and φ_R, in the laboratory frame S. The last term in this second contribution depends on the frequency dispersion and originates from the fact that the sample is receding from the source of frequency ω_I which is at rest in the laboratory frame S. This term might acquire rather large values for media with a steep frequency dispersion so as to become the leading contribution to the drag as we shall show in Sec. V.

The dragging medium induces a nonreciprocal phase shift $\Delta\phi$ that manifests itself as a small difference in the interferometer resonance frequencies for the beams propagating parallel (clockwise) and antiparallel (counterclockwise) to the velocity of the sample. Such small frequency differences are directly proportional to α_e and can easily be measured as beat frequencies in a high-precision interferometer as done, e.g., in Refs. 9 and 12. The correct determination of the phase shift across the interferometer arm length should also comprise a contribution due to the propagation in the surrounding medium whose detailed derivation is given in Appendix C. The total single-path phase shift of the beam traversing the clockwise interferometer arm length is then given by the sum of Eqs. (9) and (C4). This would clearly entail a redefinition of the drag coefficient α_e that is to be compared with experiments.

III. PHASE SHIFT AND ABSOLUTE DRAG COEFFICIENT

We now relate the measurable drag coefficient α_e to the familiar drag coefficient α_d as defined for the phase velocity of a light beam:[16,15] we will refer to the former and to the latter respectively as *effective* and *absolute* drag coefficient.

Neglecting the surrounding medium contribution the beam phase shift in the laboratory frame S can be reexpressed alternatively as

$$\Delta\phi = -s\,\mathrm{Re}[k_R] = -\frac{L}{\cos\theta_r}\frac{\omega_R}{\dfrac{c}{\mathrm{Re}[n_R]}}$$
$$\equiv -\frac{\omega_R L}{\cos\theta_r}\left(\frac{1}{\dfrac{c}{\mathrm{Re}[n_R^0]}+v\,\alpha_d\cos\varphi_R}\right), \tag{12}$$

where we purposely write the phase velocity of the beam propagating through the slab in terms of the drag coefficient α_d in much the same way as done for an infinite moving medium.[1,16,15] Since in the rest frame there is no frequency change at the sample boundaries, one has, with the help of Eqs. (6), (A4), and (A9),

$$\omega_R \simeq \omega_I[1-\beta(\cos\varphi_I\mathrm{Re}[n_I]-\cos\varphi_R\mathrm{Re}[n_R^0])]. \tag{13}$$

Using the fact that to the first order in β there is no change in the slab thickness [cf. Eqs. (1)], i.e., $L''\simeq L$, substitution of Eq. (13) into Eq. (12) yields

$$\Delta\phi = -\frac{\omega_I L''}{c}\frac{\mathrm{Re}[n_R^0]}{\cos\theta_r}+\beta\frac{\omega_I L''}{c}\frac{\mathrm{Re}[n_R^0]}{\cos\theta_r}\{\cos\varphi_I\mathrm{Re}[n_I]$$
$$+(\alpha_d-1)\cos\varphi_R\mathrm{Re}[n_R^0]\}. \tag{14}$$

By comparing this with Eq. (9) we obtain

$$\alpha_d = 1-\frac{1}{\mathrm{Re}[n_R^0]^2}+\omega_I\frac{\cos\varphi_I}{\cos\varphi_R}\frac{\mathrm{Re}[n_I]}{\mathrm{Re}[n_R^0]^2}\mathrm{Re}[\mathcal{D}_\omega]$$
$$-\frac{\tan\varphi_R}{\mathrm{Re}[n_R^0]^2}\left(\tan\theta_r+\frac{\mathrm{Re}[\mathcal{D}_\theta]}{\mathrm{Re}[n_R^0]}\right)$$
$$=1-\frac{\cos\varphi_I\mathrm{Re}[n_I]}{\cos\varphi_R\mathrm{Re}[n_R^0]}-\alpha_e\frac{\cos\theta_r}{\cos\varphi_R\mathrm{Re}[n_R^0]^2}, \tag{15}$$

where all results hold to the lowest order in the sample velocity.

In a configuration in which the slab moves in vacuum ($n_I=1$) and with velocity $\boldsymbol{v}$ parallel to the surface normal ($\theta_0=0$) and to the incident light beam ($\varphi_I=0$) one has $\varphi_R=0$ and

$$\alpha_d \to \alpha_d^{Laub} = 1 - \frac{1}{\mathrm{Re}[n_R^0]^2} + \omega_I \frac{\mathrm{Re}[\mathcal{D}_\omega]}{\mathrm{Re}[n_R^0]^2}. \tag{16}$$

This recovers exactly the form of the drag coefficient appropriate to this specific configuration that was first obtained by Laub.[23] We would then refer to α_d in Eq. (15) as the *generalized* Laub drag coefficient.

IV. DRESSED DIELECTRIC TENSOR

In the following, we will discuss in detail the dielectric tensor structure of coherently driven Cu_2O when this is used as dragging medium. The drag is experienced by a weak *probe* beam that crosses a moving sample of cuprous oxide which is in turn coherently driven by a strong *pump* beam in a typical pump-probe EIT Λ configuration.[24,25] The probe of frequency ω is tuned within the $2P$ "yellow" exciton line of frequency ω_{2P} while the pump beam of frequency ω_c is resonant with the $1S$ to $2P$ exciton transition of frequency $\omega_{2P}-\omega_{1S}$.[13,26] The dipole-forbidden $1S$ exciton state has a small linewidth ($\hbar\gamma_{1S}\simeq 0.1$ meV) compared to that of the second class allowed $2P$ exciton state ($\hbar\gamma_{2P}\simeq 1$ meV) and for a pump-beam Rabi frequency Ω_c larger or of the order of $\sqrt{\gamma_{2P}\gamma_{1S}}$, a well-developed EIT regime can be established. This entails a narrow transparency window that opens about the $2P$ exciton line with a concomitant steep dispersion.[24] From the Λ-type model Hamiltonian describing such a coherently driven system,[13] we can calculate the medium dielectric tensor which depends on the pump-beam polarization as well as on the detailed structure of the exciton levels involved. The form of the tensor will be in general anisotropic.

The pump-beam reduces in fact the cubic symmetry of Cu_2O and the form of the dielectric tensor depends on the orientation of the pump polarization with respect to the cubic axes. For a pump beam linearly polarized along [1,0,0] the system is reduced to an uniaxial crystal having x as optical c axis and similarly for a pump beam polarized along y or z. For a polarization along the diagonal [1,1,1], the system is reduced to a uniaxial crystal having [1,1,1] as c optical axis and likewise for polarizations along the other three main diagonals. Finally, for a pump beam polarized along [1,1,0] and other analogous directions, the system would be in general reduced to a biaxial crystal with optical axes along [1,1,0], [1,−1,0], and [0,0,1].

Besides general symmetry considerations, the form of the dielectric tensor further depends on the specific exciton levels. The Cu_2O conduction- and valence-band extrema occur at the Γ point (O_h point group) and have, respectively, Γ_6^+ and Γ_7^+ symmetry, each twofold-degenerate spin included.[27–29] The four states of the $1S$ exciton manifold split into an upper quadrupole allowed threefold-degenerate Γ_5^+ level and a lower forbidden nondegenerate Γ_2^+ level whose splitting Δ_S is about 12 meV. The spin degrees of freedom are strongly mixed by the spin-orbit interaction: the Γ_2^+ exciton is an optically inactive pure spin triplet, while the three degenerate Γ_5^+ states do have a spin singlet component, transforming, respectively, as yz, zx, and xy and are quadrupole allowed.[30] The 12 states of the $2P$ exciton manifold are classified according to their symmetries as follows: $\Gamma_2^+ \otimes \Gamma_4^- = \Gamma_5^-$ threefold degenerate states (pure spin triplet[31]), and $\Gamma_5^+ \otimes \Gamma_4^- = \Gamma_2^- \oplus \Gamma_3^- \oplus \Gamma_4^- \oplus \Gamma_5^-$ nine states among which only the threefold degenerate Γ_4^- states are dipole active and give rise to the second class $2P$ "yellow exciton" line.[27–29] The interactions mixing and splitting the $2P$ manifold vanish in the usual envelope function approach and are expected to be small compared to Δ_S, yet they could be significant on the scale of Rabi frequencies such that $\hbar\Omega_c \leqslant 1$ meV.

In the absence of any definite information on the fine energy structure of the $2P$ manifold, we only consider here the case in which the Γ_4^- states are well separated from the others which can then be neglected (*nondegenerate* $2P$ manifold) and the case in which the Γ_4^- states are degenerate with the others so that all nine $2P$ states, which can be equally well coupled to the Γ_5^+ $1S$ states by the pump, should be treated on equal footing (*degenerate* $2P$ manifold). Besides these two limit cases, the dielectric tensor in any other intermediate case would depend in a nontrivial way on the relations between the various splittings within the $2P$ exciton manifold and the pump Rabi frequency.

The form of the dielectric tensor for coherently driven cuprous oxide can be found for each of the two limiting cases above and a given pump polarization by a straightforward generalization[32] of the approach adopted in Ref. 13. In the following subsections we will illustrate the procedure to obtain the relevant dressed forms of the cuprous oxide dielectric tensor.

A. Nondegenerate $2P$ manifold

In this case the threefold-degenerate Γ_4^- $2P$ states, well separated from the other six states of the $2P$ manifold, are coupled to the totally symmetric ground state by a probe polarization along [1,0,0], [0,1,0], and [0,0,1] and transform, respectively, as $X=(zxp_z+xyp_y)/\sqrt{2}$, $Y=(yzp_z+xyp_x)/\sqrt{2}$, and $Z=(zxp_x+yzp_y)/\sqrt{2}$. Here, p_x, p_y, and p_z represent the $2P$ envelope functions.

A pump beam polarized, e.g., along the cubic axis [1,0,0] couples equally well the xy Γ_5^+ $1S$ state to the Y $2P$ state and the zx $1S$ state to the Z $2P$ state, whereas the X $2P$ state is unaffected by the pump. This is schematically shown in Fig. 2. The resulting dielectric tensor is uniaxial with respect to the principal axes $\hat{e}_1=[1,0,0]$, $\hat{e}_2=[0,1,0]$, and $\hat{e}_3=[0,0,1]$ with optical c axis directed along [1,0,0],

$$\epsilon_{11}=\epsilon_\parallel, \quad \epsilon_{22}=\epsilon_{33}=\epsilon_\perp, \quad \epsilon_{j\neq k}=0. \tag{17}$$

Here

$$\epsilon_\perp = \epsilon_{EIT}(\Omega_c) \equiv \epsilon_\infty + \frac{A\gamma_{2P}(\Delta - i\gamma_{1S})}{(\delta_p - i\gamma_{2P})(\Delta - i\gamma_{1S}) - \Omega_c^2/4}, \tag{18}$$

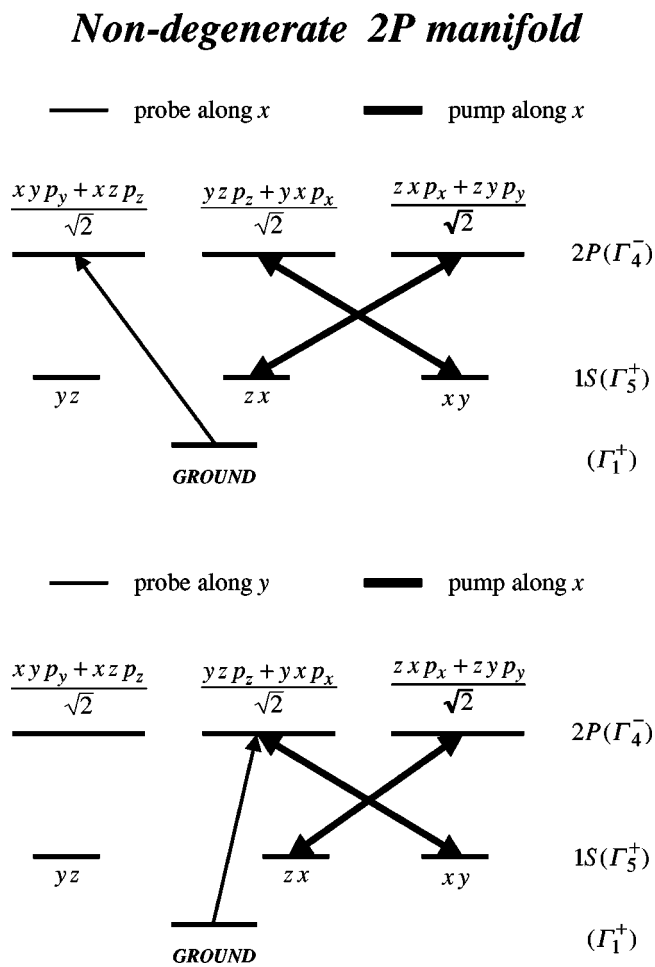

FIG. 2. Schematic diagram of the "yellow" exciton states in Cu_2O with polarizations of the pump and probe beams. The polarization of the pump beam is set along [1,0,0] and the $2P$ manifold is assumed to be nondegenerate (see text). Two choices of probe polarization are shown: only the one polarized along [0,1,0] gives rise to a Λ-type EIT configuration. A probe polarized along [0,0,1] not shown here gives also rise to a Λ-type EIT configuration.

while $\epsilon_\parallel=\epsilon_{EIT}(\Omega_c=0)$ is obtained by setting $\Omega_c\to 0$ in the above equation.[13] We denote here by $\epsilon_\infty\simeq 6.5+i2\times 10^{-3}$ the background dielectric constant while Δ is the probe and pump-beam relative detuning $(\delta_p-\delta_c)$ with $\delta_p=\omega_{2P}-\omega$ and $\delta_c=\omega_{2P}-\omega_{1S}-\omega_c$. For the yellow exciton series of bulk Cu_2O one has $\hbar\omega_{2P}\simeq 2.148$ eV and $\hbar\delta_{2P\text{-}1S}=115$ meV (Ref. 26) for the splitting while from the measured linewidth $\hbar\gamma_{2P}\simeq 1$ meV (Ref. 26) and oscillator strength[33] the coefficient A can be estimated to be $A\simeq 0.02$.[13] For the states above, the pump-beam Rabi frequency Ω_c is proportional to the $1S$-$2P$ transition dipole matrix element given by

$$\langle Y|d_x|xy\rangle=\int d\boldsymbol{r}\frac{1}{\sqrt{2}}\phi_{2Px}^*(\boldsymbol{r})ex\phi_{1S}(r)\equiv\frac{D_{21}}{\sqrt{2}}. \quad (19)$$

The expression for D_{21} is analogous to that for an atomic transition and an estimate by using hydrogenic wave functions with appropriate Bohr radii yields $D_{21}\simeq ea_B\simeq 30$ D.

We consider next a pump beam polarized along the direction [1,1,0]. Now, the xy $1S$ state is equally coupled to both the X and Y $2P$ states. In order to determine the dressed states we consider, instead of X and Y, the $2P$ states given by the symmetric combination $Y'=(X+Y)/\sqrt{2}$ and by the antisymmetric one $X'=(X-Y)/\sqrt{2}$ which is unaffected by the pump. Moreover, the Z $2P$ state is equally coupled to both the xz and yz $1S$ states. Within the present model the resulting dielectric tensor turns out to be uniaxial with respect to the principal axes $\hat{e}_1=[1,-1,0]/\sqrt{2}$, $\hat{e}_2=[1,1,0]/\sqrt{2}$, and $\hat{e}_3=[0,0,1]$ with optical c axis directed along [1,−1,0], i.e.,

$$\epsilon_{11}=\epsilon_\parallel,\quad \epsilon_{22}=\epsilon_{33}=\epsilon_\perp,\quad \epsilon_{j\neq k}=0, \quad (20)$$

where $\epsilon_\parallel$ and $\epsilon_\perp$ are the same as above.

Finally, a pump polarized along [1,1,1] couples equally well all states and the dressed states can be chosen as follows. The $2P$ state $X''=(X+Y+Z)/\sqrt{3}$ couples only to the $1S$ state $x''=(xy+zx+yz)/\sqrt{3}$ with a Rabi frequency Ω_c' proportional to $\sqrt{2/3}D_{21}$, i.e., a factor $2/\sqrt{3}$ larger than that considered above. The $2P$ state $Y''=(X-Y)/\sqrt{2}$ couples instead only to the $1S$ state $y''=(yz-zx)/\sqrt{2}$ with a Rabi frequency Ω_c'' proportional to $\sqrt{1/6}D_{21}$; the $2P$ state $Z''=(X+Y-2Z)/\sqrt{6}$ couples only to the $1S$ state $z''=(yz+zx-2xy)/\sqrt{6}$ with a Rabi frequency Ω_c'' proportional to $\sqrt{1/6}D_{21}$. The resulting dielectric tensor is uniaxial with respect to the principal axes $\hat{e}_1=[1,1,1]/\sqrt{3}$, $\hat{e}_2=[1,-1,0]/\sqrt{2}$, and $\hat{e}_3=[1,1,-2]/\sqrt{6}$ with the optical c axis directed along [1,1,1], i.e.,

$$\epsilon_{11}=\epsilon_\parallel=\epsilon_{EIT}(\Omega_c\propto\sqrt{2/3}D_{21}), \quad (21)$$

$$\epsilon_{22}=\epsilon_{33}=\epsilon_\perp=\epsilon_{EIT}(\Omega_c\propto\sqrt{1/6}D_{21}),\quad \epsilon_{j\neq k}=0, \quad (22)$$

where the form of $\epsilon_{EIT}(\Omega_c)$ is given in Eq. (18). In the last two cases of pump polarizations considered here, unlike for a pump polarized along [1,0,0], the principal axes $\hat{e}_1$, $\hat{e}_2$, and $\hat{e}_3$ are not parallel to the crystal cubic axes.

B. Degenerate $2P$ manifold

We consider next the case in which all nine $2P$ exciton states associated with the three Γ_5^+ $1S$ states are degenerate and must be treated on equal footing: xyp_x, xyp_y, xyp_z, zxp_x, zxp_y, zxp_z, yzp_x, yzp_y, and yzp_z. This is schematically shown in Fig. 3. In particular, even if the states xyp_z, zxp_y, and yzp_x are not coupled to the ground state for any polarization of the probe, they can still be coupled to the $1S$ exciton levels by the pump beam.

Now, a pump-beam polarization along [1,0,0] couples the xyp_x $2P$ state to the xy $1S$ state, the zxp_x $2P$ state to the zx $1S$ state, and the yzp_x $2P$ state to the yz $1S$ state, the other six $2P$ states being unaffected by the pump. The resulting dielectric tensor is uniaxial with the optical c axis along [1,0,0]. A probe polarized along $\hat{e}_1=[1,0,0]$ couples to the xyp_y and zxp_z $2P$ states which are unaffected by the pump and one has then

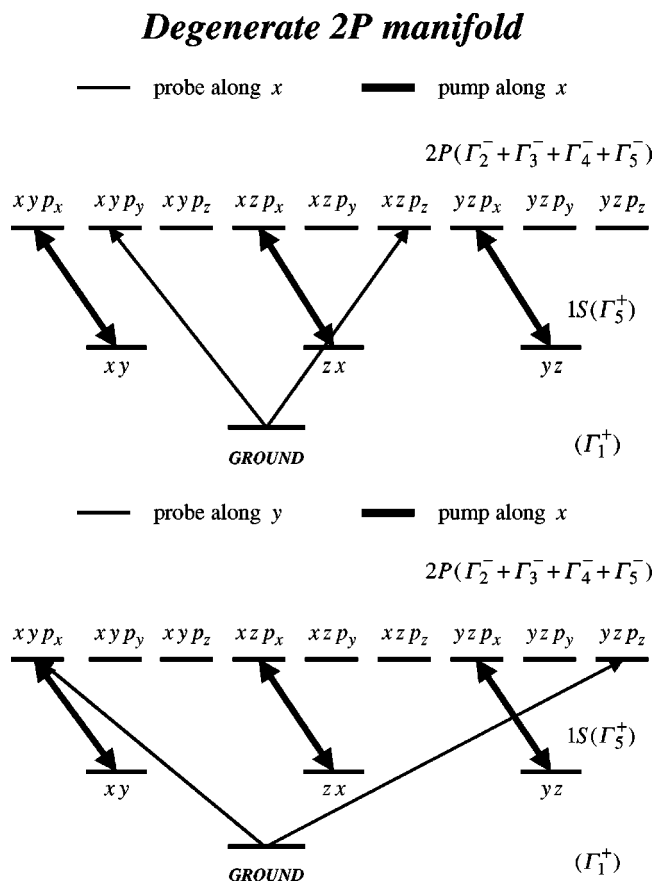

FIG. 3. Schematic diagram of the "yellow" exciton states in Cu_2O with polarizations of the probe and pump beams. The polarization of the pump beam is set along [1,0,0] and the $2P$ manifold is assumed to be degenerate. Two choices of probe polarization are shown: only the one polarized along [0,1,0] gives rise to a Λ-type EIT configuration besides a simple two-level configuration (see text) and likewise for a probe polarized along [0,0,1] not shown here.

$$\epsilon_{11}=\epsilon_{\parallel}=\epsilon_{EIT}(\Omega_c=0), \tag{23}$$

while a probe polarized along $\hat{e}_2=[0,1,0]$ couples to the yzp_z and xyp_x $2P$ states which are, respectively, unaffected and dressed by the pump so that one has instead

$$\epsilon_{22}=\epsilon_{\perp}=\frac{1}{2}[\epsilon_{EIT}(\Omega_c\propto D_{21})+\epsilon_{EIT}(\Omega_c=0)], \tag{24}$$

where the non vanishing Rabi frequency in Eq. (24) is proportional to D_{21} which is a factor of $\sqrt{2}$ larger than the one considered in Eq. (19). The same holds for a probe polarized along the other transverse direction $\hat{e}_3=[0,0,1]$ and we then have $\epsilon_{33}=\epsilon_{\perp}$ as given in Eq. (24). All off-diagonal tensor elements vanish, i.e., $\epsilon_{j\neq k}=0$.

We consider then a pump polarized along [1,1,1] for which the dressed states involve the symmetric superpositions of $2P$ states given by $(xyp_x+xyp_y+xyp_z)/\sqrt{3}$ (coupled to the xy $1S$ state), $(zxp_x+zxp_y+zxp_z)/\sqrt{3}$ (coupled to the zx $1S$ states, and $(yzp_x+yzp_y+yzp_z)/\sqrt{3}$ (coupled to the yz $1S$ state). The other $2P$ states unaffected by the pump can be chosen as $(xyp_x-xyp_y)/\sqrt{2}$, $(xyp_x+xyp_y-2xyp_z)/\sqrt{6}$, and similarly for the other four $2P$ states associated with zx and yz $1S$ states. The resulting dielectric tensor is uniaxial with the optical c axis along [1,1,1]. A probe polarized along [1,1,1] couples equally well to the six $2P$ states xyp_y, xzp_z, xzp_x, xyp_x, yzp_y, and yzp_z so that with respect to the principal axes $\hat{e}_1=[1,1,1]/\sqrt{3}$, $\hat{e}_2=[1,-1,0]/\sqrt{2}$, and $\hat{e}_3=[1,1,-2]/\sqrt{6}$ one obtains

$$\epsilon_{11}=\epsilon_{\parallel}=\frac{2}{3}\epsilon_{EIT}(\Omega_c\propto D_{21})+\frac{1}{3}\epsilon_{EIT}(\Omega_c=0). \tag{25}$$

A probe polarized along [1,−1,0] couples equally well to the four $2P$ states xyp_y, xzp_z, $-yxp_x$, and $-yzp_z$ so that one has

$$\epsilon_{22}=\epsilon_{\perp}=\frac{1}{6}\epsilon_{EIT}(\Omega_c\propto D_{21})+\frac{5}{6}\epsilon_{EIT}(\Omega_c=0). \tag{26}$$

A similar calculation can be carried out also for a probe polarized along the other transverse direction $\hat{e}_3=[1,1,-2]$, yielding $\epsilon_{33}=\epsilon_{\perp}$ as in Eq. (26) while $\epsilon_{j\neq k}=0$.

Finally, for a pump polarized along [1,1,0] the dressed states are given by the $(xyp_x+xyp_y)/\sqrt{2}$ $2P$ which is coupled to the xy $1S$ state, the $(zxp_x+zxp_y)/\sqrt{2}$ $2P$ coupled to the zx $1S$ state, and the $(yzp_x+yzp_y)/\sqrt{2}$ $2P$ coupled to the yz $1S$ state. The other $2P$ states unaffected by the pump can be chosen as $(xyp_x-xyp_y)/\sqrt{2}$, xyp_z and likewise for the other four $2P$ states associated with zx and yz $1S$ states. The resulting dielectric tensor turns out to be uniaxial with optical c axis along [1,−1,0]. A probe polarized along [1,−1,0] couples equally to xyp_y, zxp_z, $-yzp_z$, and $-xyp_x$ so that with respect to the principal axes $\hat{e}_1=[1,-1,0]/\sqrt{2}$, $\hat{e}_2=[1,1,0]/\sqrt{2}$, and $\hat{e}_3=[0,0,1]$ one has

$$\epsilon_{11}=\epsilon_{\parallel}=\epsilon_{EIT}(\Omega_c=0). \tag{27}$$

A probe polarized along [1,1,0] couples equally well to xyp_y, zxp_z, yzp_z, and xyp_x states so that

$$\epsilon_{22}=\epsilon_{\perp}=\frac{1}{2}[\epsilon_{EIT}(\Omega_c\propto D_{21})+\epsilon_{EIT}(\Omega_c=0)], \tag{28}$$

while a probe polarized along the other transverse direction $\hat{e}_3=[0,0,1]$ couples equally well to zxp_x and yzp_y states yielding $\epsilon_{33}=\epsilon_{\perp}$ as given in Eq. (28) and again with all off-diagonal elements $\epsilon_{j\neq k}=0$.

V. DRAG COEFFICIENT FOR DRESSED CUPROUS OXIDE

We now use the results for the light drag exhibited by an extra–ordinary wave in a uniaxial medium derived in Sec. II to demonstrate that a coherently driven sample of cuprous oxide used as dragging medium may improve the level of accuracy of optical drag experiments.

In the following we take a pump linearly polarized along x'', chosen to be one of the cubic axes by a suitable cleavage of the sample, which then coincides with the optical c axis.

The probe beam undergoing the phase shift impinges on the sample surface and is subsequently refracted through the medium, making an angle θ_R'' with respect to the optical c axis as shown in Fig. 1. The polarization of the probe electric field $\boldsymbol{E}''$, linear and perpendicular to the z'' axis, must be appropriate to that of an extraordinary wave in the sample rest frame S'' and must then be chosen[16,34] so that the displacement $\boldsymbol{D}''$ and electric $\boldsymbol{E}''$ fields as well as the refracted beam wave vector $\boldsymbol{k}_R''$ and optical c axis all lie on the same plane.[35] The dispersion equation for such an extraordinary probe beam polarized in the plane $x''y''$ is described by the complex refractive index

$$n_R^2(\omega_R'',\theta_R'')=\frac{\epsilon_\parallel(\omega_R'')}{1+\epsilon_r(\omega_R'')\cos^2\theta_R''}, \tag{29}$$

where

$$\epsilon_r(\omega_R'')\equiv\frac{\epsilon_\parallel(\omega_R'')}{\epsilon_\perp(\omega_R'')}-1. \tag{30}$$

The drag coefficient depends directly on the refractive index but also indirectly, i.e., through its frequency ($\mathcal{D}_\omega$) and angular ($\mathcal{D}_\theta$) derivatives, so that, when Eq. (29) is substituted into Eq. (9) or (15), the resulting drags will depend on the two tensor components $\epsilon_\parallel(\omega_R'')$ and $\epsilon_\perp(\omega_R'')$. These depend in turn on the choice of the pump-beam polarization as well as on the specific exciton level structure.

We proceed by giving a detailed discussion of the drag coefficient for the case of a *nondegenerate* $2P$ exciton manifold and a pump polarized along [1,0,0]. The relevant dielectric tensor as given in Eqs. (17), (18), and (19) can be put in the matrix form

$$\begin{pmatrix} \epsilon_{EIT}(\Omega_c=0) & 0 & 0 \\ 0 & \epsilon_{EIT}\left(\Omega_c\propto\frac{D_{21}}{\sqrt{2}}\right) & 0 \\ 0 & 0 & \epsilon_{EIT}\left(\Omega_c\propto\frac{D_{21}}{\sqrt{2}}\right) \end{pmatrix}. \tag{31}$$

Unlike in the absence of the pump for which $\epsilon_r=0$, the terms of α_e involving the reduced dielectric function ϵ_r will in general not vanish when Eqs. (17) and (18) are substituted into Eq. (9), some terms acquiring smaller values than others for probe frequencies within the transparency bandwidth. With the pump exactly on resonance ($\delta_c=0$), $\mathrm{Re}[\epsilon_r]$ as well as the frequency derivatives of $\mathrm{Im}[\epsilon_\parallel]$ and $\mathrm{Im}[\epsilon_r]$ takes on vanishingly small values within this bandwidth so that for probe detunings up to several tenths of γ_{2P} a more compact form of the drag can be obtained after setting these terms to zero in α_e. The resulting form of drag can be further simplified, observing that in the same detuning range the remaining variables are nearly constant and acquire fairly larger values but still less than unity (10^{-3}–10^{-2}) and increase according to $|\mathrm{Im}[\epsilon_r]|<\gamma_{2P}|\partial_\omega\mathrm{Re}[\epsilon_r]|\leqslant\mathrm{Im}[\epsilon_\parallel]\leqslant\gamma_{2P}|\partial_\omega\mathrm{Re}[\epsilon_\parallel]|$. It is then possible to carry out a successive series expansion of α_e with respect to $\mathrm{Im}[\epsilon_r]$, $\gamma_{2P}\partial_\omega\mathrm{Re}[\epsilon_r]$, and $\mathrm{Im}[\epsilon_\parallel]$ so that after some algebra we obtain, to the lowest order,

$$\begin{aligned}\alpha_e\simeq&-\frac{\cos\varphi_I}{\cos\theta_r}\left(\mathrm{Re}[n_I]\sqrt{\mathrm{Re}[\epsilon_\parallel]}-\frac{\cos\varphi_R}{\cos\varphi_I}\right)+\sin\varphi_R\frac{\tan\theta_r}{\cos\theta_r}\\&-\frac{\omega_I}{2}\frac{\cos\varphi_I}{\cos\theta_r}\frac{\mathrm{Re}[n_I]}{\sqrt{\mathrm{Re}[\epsilon_\parallel]}}\left(\frac{\partial\mathrm{Re}[\epsilon_\parallel]}{\partial\omega_I}-\mathrm{Re}[\epsilon_\parallel]\right.\\&\left.\times\cos^2\theta_R\frac{\partial\mathrm{Re}[\epsilon_r]}{\partial\omega_I}\right).\end{aligned} \tag{32}$$

Higher order contributions containing terms proportional to the product of $\mathrm{Im}[\epsilon_r]$,$\mathrm{Im}[\epsilon_\parallel]$, $\gamma_{2P}\partial_\omega\mathrm{Re}[\epsilon_\parallel]$ and of $\mathrm{Im}[\epsilon_r]$, $\gamma_{2P}\partial_\omega\mathrm{Re}[\epsilon_r]$, $\mathrm{Im}[\epsilon_\parallel]$ have been neglected and the frequency dependences of all dielectric functions are not explicitly indicated. The refracted angle θ_r as well as θ_R and φ_R, which determine the orientation of the refracted beam path through the moving sample as observed in S, can all be determined from the law of refraction for uniaxial crystals[16] and from the aberration law[15] once the incident beam geometry in the laboratory frame S is known.

The drag comprises four contributions whose origin has

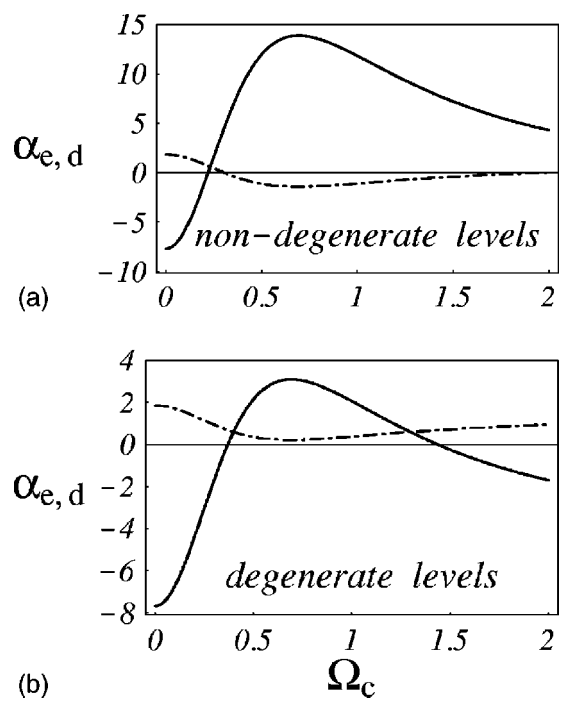

FIG. 4. Effective α_e (solid line) and absolute α_d (dot-dashed line) drag coefficients for a resonant probe and a resonant pump beam of variable Rabi frequency Ω_c. The pump beam is polarized along the direction [1,0,0] in both cases of *nondegenerate* (upper frame) and *degenerate* (lower frame) exciton levels. We take the surrounding medium to be the vacuum ($n_I=1$) and the cleavage angle $\alpha=3°$ while the incident beam geometry is such that $\varphi_I=40°$ and $\theta_0=5°$. The refracted angle is $\theta_r=16°$ from which in turn the values of φ_R and θ_R can be obtained. All frequencies are given in units of γ_{2P} ($\hbar\gamma_{2P}=1$ meV).

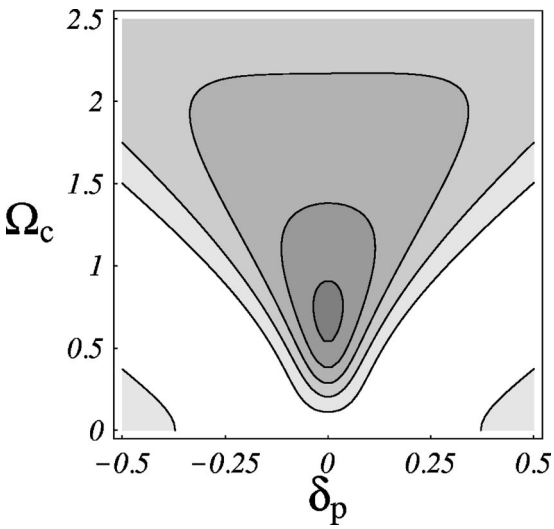

FIG. 5. Effective drag coefficient α_e exhibited by a probe sweeping the exciton resonance region and a resonant pump beam of variable Rabi frequency Ω_c and polarized along [1,0,0]. The exciton levels are *nondegenerate* with $\hbar\gamma_{1S}=0.1$ meV and $A=0.02$. Contour lines determine the detunings δ_p and the Rabi frequencies Ω_c yielding a fixed value of the drag and darker regions correspond to points of larger drags. Moving outward from the darkest center region where $\alpha_e^{max}\simeq 14$, the first open contour line corresponds to values of δ_p and Ω_c for which the drag vanishes and marks the transition from positive (inside) to negative (outside) drag values. Notation, units and parameters are otherwise the same as in Fig. 4.

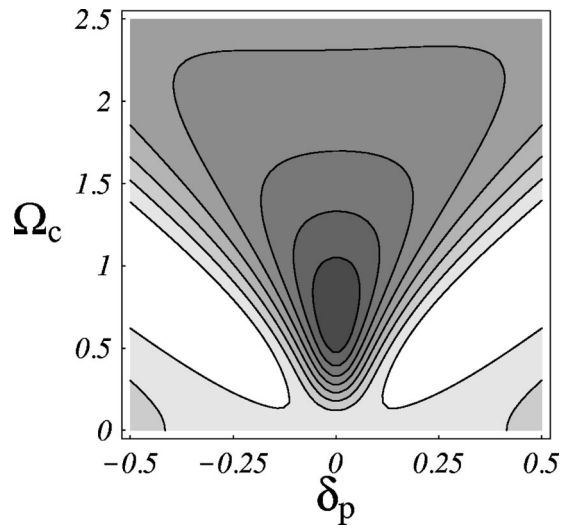

FIG. 6. Same as in Fig. 5 with $\hbar\gamma_{1S}=0.1$ meV and $A=0.04$. In the dark center region the drag reaches the maximum value $\alpha_e^{max}\simeq 22$.

been thoroughly discussed below Eq. (9). Their magnitudes may be controlled directly by varying the intensity of the pump beam (Ω_c) and the incident beam geometry (φ_I,θ_0) so that the drag may acquire positive and negative values or it may even vanish. The first two terms on the right-hand side of Eq. (32) are typically of the same order of magnitude and in fact much smaller than the last two in the brackets which are the dominant contributions when dispersion is important. For appropriate choices of Ω_c's and θ_R's these two terms may just become comparable in magnitude so as to make the overall drag to vanish at probe frequencies which are determined by the specific choice of pump and incident beam parameters. The second of these terms, in particular, is a direct consequence of the symmetry breaking induced by the external pump beam and does not appear in the absence of the pump beam as in this case one has $\epsilon_\parallel=\epsilon_\perp$ and $\epsilon_r=0$.

For a resonant probe and a set incident beam geometry, there exists in general a pump intensity at which α_e vanishes. This is shown in Fig. 4 where we report numerical results obtained from Eqs. (32), (30), and (31) for a *nondegenerate* $2P$ exciton manifold. The case of a nonresonant probe is instead shown in Figs. 5, 6, and 7 where α_e is seen to vanish for increasing pump-beam intensities in the narrow resonance region $|\delta_p|<0.5\gamma_{2P}$. Conversely, in the absence of the pump-beam the drag can never be observed to vanish in Figs. 5, 6, and 7: in this case the frequency dependence of α_e can no longer be tailored but is just fixed by the material parameters.

For the same incident beam geometry there exists a small range of detunings and pump intensities, represented by the darkest central region in Figs. 5, 6, and 7, for which the drag reaches its maximum value $\alpha_e^{max}\simeq 14$. Large values of the drag arise from the steep frequency dispersion[14] occurring at resonance where absorption is, however, largely quenched by quantum interference.[13] The large values of the dispersion and of the absorption quenching originate in turn from a large effect of electromagnetically induced transparency in the $2P$ exciton resonance region.

Both exciton dephasing (γ_{1S}) and transition oscillator strength ($\propto A$) play no essential role in the vanishing of the drag but are instead crucial in determining its largest value. This is shown in Figs. 5, 6, and 7 where reducing γ_{1S} to half its current value or making A twice as large would produce approximately a 50% increase[36] in the magnitude of α_e.

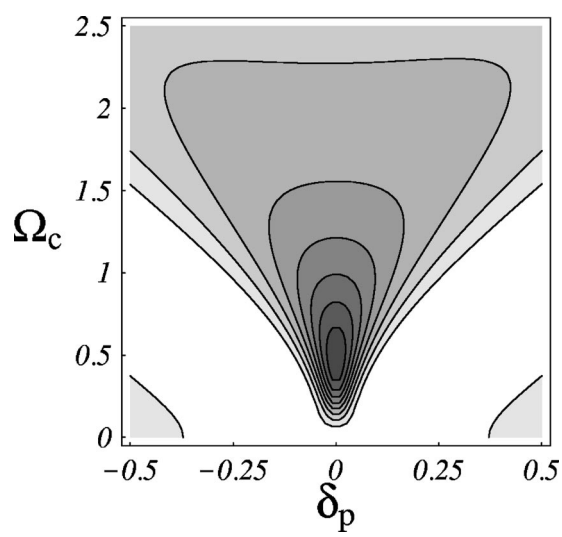

FIG. 7. Same as in Fig. 5 with $\hbar\gamma_{1S}=0.05$ meV and $A=0.02$. In the dark center region the drag reaches the maximum value $\alpha_e^{max}\simeq 23$.

Note that the large drag values obtained here are at least one order of magnitude larger than those obtained, e.g., with glass media[12] and at least twice as large as those[37] that one would obtain with Cu_2O in the absence of the pump beam. Because the interferometer frequency beat depends on the product $\beta\times\alpha_e$,[9,12] a large α_e improves the drag measurement accuracy by enhancing the sensitivity of the interferometer at low velocities of the dragging medium.

We also show in Figs. 4(a) and 8 the absolute drag coefficient α_d for a *nondegenerate* $2P$ exciton manifold. A simple expression for α_d can be derived by using the same approximations used to derive Eq. (32). Unlike α_e, this is seen to vanish around resonance for a weak as well as for fairly large values of the pump-beam intensity. Stronger beams, in particular, would enable one to make α_d to vanish over almost the whole transparency region with a concomitant higher degree of transparency.[13] Exciton dephasing and oscillator strength would affect α_d in much the same way as they affect α_e and will not be discussed here.

For the specific cases discussed here any two observers respectively in S and S'' and in relative motion with respect to one another would then observe the *same* refractive index and this would hold for all velocity of experimental interest.

We finally illustrate dragging effects for the case of a *degenerate* $2P$ exciton manifold. The relevant dielectric tensor given in Eqs. (23) and (24) may be written in the form

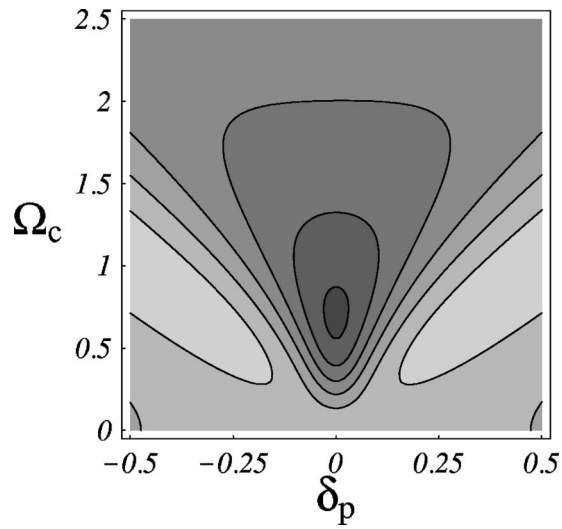

FIG. 8. Absolute drag coefficient α_d as a function of the probe detuning δ_p and for a pump beam of variable Rabi frequency Ω_c. The exciton levels are *nondegenerate* with $\hbar\gamma_{1S}=0.1$ meV and $A=0.02$ while the pump beam is resonant and polarized along [1,0,0]. The third closed contour-line profile from the center corresponds to values of δ_p and Ω_c for which α_d vanishes and marks the transition from negative (inside) to positive (outside) values of the drag. Notation, units and parameters are otherwise the same as in Fig. 4.

$$\begin{pmatrix} \epsilon_{EIT}(\Omega_c=0) & 0 & 0 \\ 0 & \dfrac{\epsilon_{EIT}(\Omega_c\propto D_{21})}{2}+\dfrac{\epsilon_{EIT}(\Omega_c=0)}{2} & 0 \\ 0 & 0 & \dfrac{\epsilon_{EIT}(\Omega_c\propto D_{21})}{2}+\dfrac{\epsilon_{EIT}(\Omega_c=0)}{2} \end{pmatrix} \tag{33}$$

and the same approximations used for the nondegenerate case apply here. An analogous simple form for the effective and absolute drag can be derived leading to the quantitative results shown in Figs. 4 and 9. We will not examine here how the dephasing and the oscillator strength would affect α_e or how α_d would depend on the pump intensity as done before. Considerations similar to those following Eq. (32) hold essentially unchanged also for the degenerate case. We must, however, note that, unlike for the nondegenerate Γ_4^- excitons states, α_e turns out to be generally smaller in magnitude whereas for a resonant probe α_d may become very small yet without vanishing.

VI. CONCLUSIONS

We have developed a general theory of the Fresnel-Fizeau light drag for nonstationary boundaries and one in which frequency and angular dispersion of the dragging medium are both included. Unlike in an isotropic material, where the dispersion relations are independent of the direction $\boldsymbol{k}$ of the wave propagation, in a uniaxial medium the dispersion relations depend on the angle between $\boldsymbol{k}$ and the optical c axis. Besides the familiar contribution ($\mathcal{D}_\omega$) due to the medium frequency dispersion, Eq. (9) encompasses then a new term ($\mathcal{D}_\theta$) which stems from the medium anisotropy. This expression for the light drag, which is one of our main results, further embodies effects of sample tilting (θ_0) and of the associated refraction. Such effects give rise to a beam-path misalignement (φ_I) and to a beam-path aberration originating from changes between the laboratory and sample rest frames which are commonly not fully accounted for. The beam-path aberration contribution, essentially proportional to the tangent term on the right-hand side of Eq. (9), and that associated with the medium anisotropy ($\mathcal{D}_\theta$) are independent

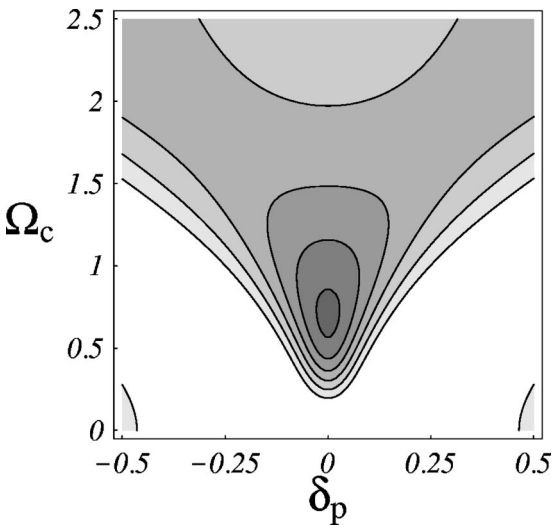

FIG. 9. Same as in Fig. 8 for the case of *degenerate* exciton levels. The third closed contour-line profile from the center corresponds to values of δ_p and Ω_c for which the drag vanishes and marks the transition from positive (inside) to negative (outside) values of the drag.

of one another, yet they are both absent for light beams dragged in the direction of the sample velocity and of its surface normal.[14] In a realistic drag measurement scenario sample tilts are, however, needed to avoid multiple internal reflections and to minimize the effect of backreflections of light into the interferometer beam path. Corrections associated with sample tilts should therefore be taken into the proper account by the theory in order to minimize the discrepancy between theory and experiment and hence to improve precision in the measurement of the Fresnel light drags.

We have further devised a Fizeau-type optical interferometer that uses as dragging medium a slab of coherently driven cuprous oxide (Cu_2O) in a typical pump-probe configuration[13] rather than glass media.[12] We have considered two possible exciton level structures in which the Λ-type EIT configuration can be implemented and we have derived explicit expressions for the relevant form of the dressed dielectric tensor which are anisotropic and which depend on the direction of the pump polarization with respect to the crystal cubic axes. The material parameters determining the dressed dielectric tensor, in particular the linewidth and the oscillator strength of the various transitions involved, have been taken from experiments.[26,34] Our general theory for the Fresnel-Fizeau light-drag experienced by the probe beam indicates that the observation of either large or vanishing drags should be favored around the "yellow" $2P$ exciton resonance region where dispersion is rather steep, absorption is largely quenched by quantum interference, and where the sample may be rendered uniaxial by a proper choice of the pump polarization.

Our situation, unlike most familiar light-drag experiments[3,6,7] where the leading contribution to the drag is determined by the refractive index of the medium and dispersion is not a substantial correction, resembles much more to that of neutrons in matter where the dispersive contribution can compare with or even exceed the other.[39] Matter waves and light waves in moving media share another and crucial feature, i.e., the fact that the drag may vanish. This means that no change in the phase velocity of light propagating through the moving medium is observed with respect to light propagating through the medium at rest. This somewhat surprising conclusion holds in this case for all velocities of experimental interest and originates from the fact that $\epsilon_\parallel$ and ϵ_r in Eq. (32) have the same sign dispersion and comparable magnitudes about resonance so as to cancel with one another (see Fig. 4, Figs. 5, 6, and 7, Fig. 8, and Fig. 9). Null drags have so far been observed for thermal neutrons traversing a moving medium contained inside stationary boundaries and exhibiting no nuclear resonance.[38,39] While it follows as a general result[38] that no neutron Fizeau effect occurs for an off-resonance neutron probe and boundaries at rest, it is here worthwhile to note that in our case a null effect is instead exhibited for a resonant light probe and moving boundaries. The null result depends in one case on the specific form of the dispersion relation for neutrons in material media,[39] while on the other it depends both on the EIT dispersion and on the induced anisotropy of light waves in cuprous oxides.

Our work aims both to improve the theoretical predictions of the drag coefficient by including corrections that are not commonly accounted for and to improve the level of accuracy of optical drag measurements by devising a scheme which enhances the interferometer sensitivity at low dragging velocities. The corrections that we anticipate will further endeavor to improve the theory's predictions for light propagating in moving media.

The present treatment is adequate for a monochromatic light probe beam impinging on a sample moving with constant and uniform velocity. Extensions to include for continuous-mode narrow-band coherent probes as well as for accelerated motion and nonuniform velocity profiles are certainly most interesting. This would comprise, in particular, a rotating sample configuration where tunable light drags may provide a precision bias source in rotation sensor devices. Such extensions greatly complicate the derivations carried out here, and they are reserved for future work.

ACKNOWLEDGMENTS

We are grateful to S. Harris and E. Arimondo for a critical reading of the manuscript and stimulating discussions over the various stages of the work. We greatly acknowledge support by the INFM and the European Community (Contract No. HPRICT1999-00111).

APPENDIX A

We derive in this appendix an approximate expression for the laboratory frame refractive index $n_R[\omega_R, \theta_R]$. We start by using the property that $k^2 - \omega^2/c^2$ is an invariant under the combined Lorentz transformation (1). This may directly be checked with the help of Eqs. (1): namely,

$$k_R''^2 \equiv k_{R,x}''^2 + k_{R,y}''^2 + k_{R,z}''^2 = k_{R,y}''^2 + k_{R,z}''^2 + \gamma^2\left(k_{R,x}''^2 + \beta^2\frac{\omega_R^2}{c^2} - 2\beta\frac{\omega_R k_{R,x}}{c}\right) \tag{A1}$$

and

$$\frac{\omega_R''^2}{c^2} = \gamma^2\frac{\omega_R^2}{c^2} + \gamma^2\beta^2 k_{R,x}''^2 - 2\beta\gamma^2\frac{\omega k_{R,x}}{c} \tag{A2}$$

and, hence,

$$k_R''^2 - \frac{\omega_R''^2}{c^2} = k_{R,y}^2 + k_{R,z}^2 + \gamma^2(1-\beta^2)k_{R,x}^2 + \gamma^2\frac{\omega_R^2}{c^2}(\beta^2-1) = k_R^2 - \frac{\omega_R^2}{c^2}, \tag{A3}$$

where momenta and frequencies refer to those inside the medium. It follows from Eq. (A3) and the first-order Doppler shift

$$\omega_R'' \simeq \omega_R\{1-\beta\cos\varphi_R \mathrm{Re}[n_R(\omega_R,\theta_R)]\} \tag{A4}$$

that

$$k_R''^2 = k_R^2 + \frac{\omega_R''^2 - \omega_R^2}{c^2} \simeq k_R^2 - 2\beta\cos\varphi_R\frac{\omega_R^2}{c^2}\mathrm{Re}[n_R(\omega_R,\theta_R)]. \tag{A5}$$

Since the magnitude of the real part of the beam wave vector $\boldsymbol{k}_R$, for which the Lorentz transformation (1) is defined, is $k_R = |\boldsymbol{k}_R| = \omega_R \mathrm{Re}[n_R(\omega_R,\theta_R)]/c$, one has

$$k_R'' \simeq k_R\left(1-\beta\frac{\cos\varphi_R}{\mathrm{Re}[n_R(\omega_R,\theta_R)]}\right). \tag{A6}$$

Thus from Eqs. (A4) and (A6) one has

$$\frac{\omega_R''}{k_R''} \simeq \frac{\omega_R\{1-\beta\cos\varphi_R\mathrm{Re}[n_R(\omega_R,\theta_R)]\}}{k_R\left(1-\beta\frac{\cos\varphi_R}{\mathrm{Re}[n_R(\omega_R,\theta_R)]}\right)} \simeq \frac{\omega_R}{k_R} - \beta c\cos\varphi_R\left(1-\frac{1}{\mathrm{Re}[n_R(\omega_R,\theta_R)]^2}\right), \tag{A7}$$

which is the usual transformation law for the phase velocity of a light wave propagating through an infinite moving medium and which yields, in turn,

$$\frac{1}{\mathrm{Re}[n_R(\omega_R'',\theta_R'')]} \simeq \frac{1}{\mathrm{Re}[n_R(\omega_R,\theta_R)]} - \beta \times\cos\varphi_R\left(1-\frac{1}{\mathrm{Re}[n_R(\omega_R,\theta_R)]^2}\right). \tag{A8}$$

To the lowest order in β, the reverse transformation obtains by interchanging $n_R(\omega_R'',\theta_R'') \leftrightarrow n_R(\omega_R,\theta_R)$ and $\beta \leftrightarrow -\beta$ so that solving for $\mathrm{Re}[n_R(\omega_R,\theta_R)]$ in Eq. (A8) one obtains, with the help of Eqs. (5), (6), and (8) after straightforward iteration,

$$\begin{aligned}\mathrm{Re}[n_R(\omega_R,\theta_R)] &\simeq \mathrm{Re}[n_R(\omega_R'',\theta_R'')] - \beta\cos\varphi_R\{\mathrm{Re}[n_R(\omega_R'',\theta_R'')]^2 - 1\}\\ &\simeq \mathrm{Re}[n_R^0(\omega_I,\theta_R)] + \beta\cos\varphi_R\{1 - \mathrm{Re}[n_R^0(\omega_I,\theta_R)]^2\}\\ &\quad - \beta\left(\omega_I\cos\varphi_I\mathrm{Re}[n_I(\omega_I)]\mathrm{Re}[\mathcal{D}_\omega] - \frac{\sin\varphi_R\mathrm{Re}[\mathcal{D}_\theta]}{\mathrm{Re}[n_R^0(\omega_I,\theta_R)]}\right).\end{aligned} \tag{A9}$$

Here $n_R^0(\omega_I,\theta_R)]$ represents the lowest-order contribution to the *actual* refractive index $n_R(\omega_R,\theta_R)]$ of the sample in the laboratory frame S.

APPENDIX B

We now provide an alternate derivation of $\Delta\phi$ that is aimed to clarify the physics underlying the different contributions to the light drag. The derivation sheds light on the physics of a contribution, in particular, which arises from the fact that both incident and refracted beams suffer aberration and which is not commonly accounted for. The form of such a contribution does not depend on the specific nature of the ordinary or extraordinary mode propagating in an uniaxial medium and the more straightforward derivation for an *ordinary* mode will be presented here.

The incident and refracted angles θ_i and θ_r are to be connected through the appropriate form of the Snell's law for a moving interface and this is best obtained by first giving the Snell's law in the rest frame S''. Matching the phase of the incident beam,

$$\mathrm{Re}[\mathbf{k}_I'']\cdot\mathbf{r}_\parallel'' = \mathrm{Re}[k_I'']\hat{\mathbf{k}}_I''\cdot\mathbf{r}_\parallel'' = \frac{\omega_I''}{c}\mathrm{Re}[n_I(\omega_I'')]r_\parallel''\cos\left(\frac{\pi}{2}-\theta_i''\right) \tag{B1}$$

and the phase of the refracted beam, for which a similar expression holds, on both sides of the two media common boundary yields the required equation in the form

$$\sin\theta_r'' = \frac{\mathrm{Re}[n_I(\omega_I'')]}{\mathrm{Re}[n_R(\omega_R'')]}\sin\theta_i''. \tag{B2}$$

The index of refraction $n_R(\omega_R'') \to \sqrt{\epsilon_\perp(\omega_R'')}$ does not depend here on the angle θ_R'' between the ordinary beam refracted wavevector and the optical c axis.[16] Using

$$\theta_i'' \simeq \theta_i + \frac{\beta\sin\varphi_I}{\mathrm{Re}[n_I(\omega_I)]}, \tag{B3}$$

and the appropriate forms of Eqs. (5) and (8) as well as a suitable expansion for $n_I(\omega_I'')$, which can be obtained as in Eq. (A8) through the transformation law of the phase velocity in an infinite medium, we obtain, after expanding both sides of Eq. (B2),

$$\sin\theta_i \simeq \frac{\mathrm{Re}[n_R^0]}{\mathrm{Re}[n_I]}\sin\theta_r + \beta\frac{\Delta_{Snell}}{\mathrm{Re}[n_I]}, \tag{B4}$$

where

$$\Delta_{Snell} = \cos(\theta_0+\varphi_I+\varphi_R)\sin(\varphi_R-\varphi_I)+\cos\varphi_I\{\sin\theta_i(1 - \mathrm{Re}[n_I]^2) - \omega_I\sin\theta_r\mathrm{Re}[n_I]\mathrm{Re}[\mathcal{D}_\omega]\}. \tag{B5}$$

The shorthand notation used in Eq. (9) is herewith resumed and $n_R^0=\sqrt{\epsilon_\perp(\omega_I)}$ is the lowest-order contribution to the laboratory frame sample refractive index.

We modify the derivation of Eq. (9) by using a different expression for θ_r'' in the numerator and denominator of Eq. (3). This can be obtained by following essentially the same procedure used to go from Eq. (B2) to Eq. (B4) except that we now expand only the right-hand side of Eq. (B2): namely,

$$\theta_r'' \simeq \arcsin\mathcal{S} + \frac{\beta}{(1-\mathcal{S}^2)^{1/2}}\left(\frac{\sin\varphi_I\cos\theta_i}{\mathrm{Re}[n_R^0]}\right) - \frac{\beta\mathcal{S}}{(1-\mathcal{S}^2)^{1/2}}\cos\varphi_I\left(\frac{1-\mathrm{Re}[n_I^2]}{\mathrm{Re}[n_I]} - \omega_I\frac{\mathrm{Re}[n_I\mathcal{D}_\omega]}{\mathrm{Re}[n_R^0]}\right), \tag{B6}$$

where

$$\mathcal{S} \equiv \sin\theta_i\mathrm{Re}[n_I]/\mathrm{Re}[n_R^0]. \tag{B7}$$

Substituting Eq. (B6) instead of θ_r'' obtained from Eq. (8) in the original expression (3) while proceeding otherwise in the same way through the derivation of Eq. (9) we obtain

$$\Delta\phi = -\frac{\omega_I L''}{c}\frac{\mathrm{Re}[n_R^0]}{(1-\mathcal{S}^2)^{1/2}} - \beta\frac{\omega_I L''}{c(1-\mathcal{S}^2)^{1/2}} \times\{\cos(\arcsin\mathcal{S}-\theta_0) - \cos\varphi_I\mathrm{Re}[n_I](\mathrm{Re}[n_R^0] + \omega_I\mathrm{Re}[\mathcal{D}_\omega])\} - \beta\frac{\omega_I L''\mathcal{S}}{c(1-\mathcal{S})^{3/2}}\left[\cos\theta_i\sin\varphi_I + \sin\theta_i\cos\varphi_I\left(1-\mathrm{Re}[n_I]^2 - \frac{\omega_I\mathrm{Re}[\mathcal{D}_\omega]\mathrm{Re}[n_I]^2}{\mathrm{Re}[n_R^0]}\right)\right]. \tag{B8}$$

This shift comprises two velocity-dependent terms the second of which is proportional to $\mathcal{S}/(1-\mathcal{S})^{-3/2}$ and originates solely from the velocity dependence of the angle θ_r''. This second term would be missing if we had used only the velocity-independent contribution on the right-hand side of Eq. (B6). If we next use Eq. (B4) to iterate Eq. (B8) for θ_i we obtain, after some lengthly but straightforward algebra,

$$\Delta\phi = -\frac{\omega_I L''}{c}\frac{\mathrm{Re}[n_R^0]}{\cos\theta_r} - \beta\frac{\omega_I L''}{c}\frac{1}{\cos\theta_r}\{\cos\varphi_R - \cos\varphi_I\mathrm{Re}[n_I](\mathrm{Re}[n_R^0]+\omega_I\mathrm{Re}[\mathcal{D}_\omega])\} + \beta\frac{\omega_I L''}{c}\frac{\sin\theta_r}{\cos^3\theta_r}\left[\frac{\sin\theta_0 - \sin(\theta_r+\varphi_R)}{2}\right], \tag{B9}$$

which reduces, upon some simple trigonometry, exactly to Eq. (9) when the angular dependence of the refractive index is neglected. The above procedure confirms the result (9) and furthermore shows that the last term on the right-hand side of Eq. (B9) is solely related to the velocity-dependent contribution to the beam orientation θ_r'' through the sample. Such a term is due to the fact that both incident and refracted beams suffer aberration upon being boosted from S to S'' and should therefore appear in the theoretical expression of the drag when aberration of both incident and refracted beams are accounted for.

The refracted angle $\tilde{\theta}_r$ experienced by a beam of frequency ω_I and incident at an angle θ_i on a slab *at rest* is given by Eq. (B7), i.e., $\tilde{\theta}_r = \arcsin\mathcal{S}$. For a slowly moving sample the correct refracted angle θ_r should instead be determined as a solution of Eq. (B4). For small velocities, however, θ_r will not differ much from $\tilde{\theta}_r$ so that, upon inverting Eq. (B4), we can expand θ_r around $\tilde{\theta}_r$ and one obtains, to first order in β,

$$\theta_r \simeq \tilde{\theta}_r - \beta\frac{\Delta_{Snell}[\tilde{\theta}_r]}{\cos\tilde{\theta}_r\mathrm{Re}[n_R^0]}. \tag{B10}$$

The factor multiplying β on the right-hand side of Eq. (B10) is typically not large enough to induce significant velocity-dependent corrections to the value of $\tilde{\theta}_r$. For the Cu_2O parameters relevant to the tensor component (18) and typical cm/sec dragging speeds,[12] departures of θ_r from $\tilde{\theta}_r$ in Eq. (B10) turn out to be of the order of 10^{-12} so that incident and refracted angles through the moving sample may be related, to a very good approximation, by Snell's law as if the sample were to be at rest.

APPENDIX C

In this appendix we evaluate the phase shift of the optical beam due the surrounding medium that is typically taken to be air.[12] As seen in the laboratory frame S, the air-filled part of the arm interferometer induces the shift

$$\Delta\phi_{air} = -(s_{in}+s_{out})\mathrm{Re}[k_I] = \Delta\phi_{air}^{cav} - \Delta\phi_{ia}, \tag{C1}$$

where

$$\Delta\phi_{air}^{cav} = -s\mathrm{Re}[k_I] = -\frac{\omega_I\mathrm{Re}[n_I(\omega_I)]}{c}\frac{D}{\cos\varphi_I} \tag{C2}$$

is the fixed shift across the arm length D experienced by a beam incident at an angle φ_I in the absence of the slab (Fig. 1). The difference between Eq. (C2) and the combined phase

shifts along the incident (s_1) and emerging (s_2) beams can be evaluated in much the same way as done in Eq. (3): namely,

$$\Delta\phi_{ia}=(k_I''^{\mu}\Delta x''_{ia\mu})\big|_{\Delta t=0}=-\beta\frac{\omega_I''}{c}(x_a-x_i)-s''_{air}\mathrm{Re}[k_I'']$$
$$=-\frac{\omega_I''L''}{c}\frac{\cos\varphi_R''}{\cos(\theta_0+\varphi_R'')}\left(\beta+\frac{\mathrm{Re}[n_I(\omega_I'')]}{\cos\varphi_I''}\right). \qquad \text{(C3)}$$

This clearly depends on the inclination of the beam path across the sample and is then velocity dependent; s''_{air} is the optical beam path length in air which complements the phase shifts of the incident (s''_{in}) and emerging (s''_{out}) beams to yield the total shift across the arm length D (see Fig. 1). Upon using Eq. (6), the appropriate expressions for the aberration of φ_I'' and φ_R'' and the expansion of $\mathrm{Re}[n_I(\omega_I'')]$ similar to that obtained in Eq. (A8), we arrive at

$$\Delta\phi_{air}\simeq-\frac{\omega_I}{c}\frac{\mathrm{Re}[n_I(\omega_I)]}{\cos\varphi_I}\left(D-L''\frac{\cos\varphi_R}{\cos\theta_r}\right)+\beta\frac{\omega_I L''}{c}\frac{\cos\varphi_R}{\cos\theta_r}$$
$$\times\left[\tan^2\varphi_I+\sin\theta_0\frac{\mathrm{Re}[n_I]}{\mathrm{Re}[n_R^0]}\frac{\tan\varphi_R}{\cos\theta_r\cos\varphi_I}\right]. \qquad \text{(C4)}$$

The first term on the right is the phase shift for a stationary sample while the last one arises from the sample motion and is solely due to the inclusion of the aberration suffered by both incident and refracted beams when boosted from S to S''.

[1] A. Fresnel, Ann. Chim. Phys. **9**, 57 (1818); **9**, 286 (1818).

[2] W. Rosser, *An Introduction to the Theory of Relativity* (Butterworths, London, 1964), Chap. 2.

[3] H. Fizeau, C. R. Hebd. Seances Acad. Sci. **33**, 349 (1851); Ann. Chim. Phys. **57**, 385 (1859).

[4] M. von Laue, Ann. Phys. (Leipzig) **23**, 989 (1907).

[5] A. Michelson, Am. J. Sci. **22**, 20 (1881); A. Michelson and E. Morley, *ibid.* **34**, 333 (1881).

[6] A. Michelson and E. Morley, Am. J. Sci. **31**, 377 (1886).

[7] P. Zeeman, Proc. R. Acad. Sci. Amsterdam **17**, 445 (1914).

[8] P. Zeeman, Proc. R. Acad. Sci. Amsterdam **23**, 1402 (1922).

[9] W. Macek *et al.*, J. Appl. Phys. **35**, 2556 (1964).

[10] H. Bilger and T. Zavodny, Phys. Rev. A **5**, 591 (1972); H. Bilger and W. Stowell, *ibid.* **16**, 313 (1977).

[11] The idea of using a rotating disk was originally suggested and examined by Lodge who, however, deemed impractical its experimental realization owing to the current state of the art [O. Lodge, Philos. Trans. R. Soc. London, Ser. A **184**, 727 (1893)].

[12] G.A. Sanders and Ezeckiel, J. Opt. Soc. Am. B **5**, 674 (1988) and references therein.

[13] M. Artoni, G.C. La Rocca, and F. Bassani, Europhys. Lett. **49**, 445 (2000).

[14] See M. Artoni *et al.*, Phys. Rev. Lett. **86**, 2549 (2001). We here examined the case of a probe beam propagating parallel to the sample velocity and to its surface normal, a simplified configuration which omits angular aberrations altogether.

[15] J. Jackson, *Classical Electrodynamics*, 2nd ed. (Wiley, New York, 1975), Chap. 11.

[16] L.D. Landau and E.M. Lifschitz, *Electrodynamics of Continuous Media* (Pergamon Press, Oxford, 1960), Chap. 78.

[17] In some optical Fresnel-Fizeau experiments the dragging medium moves sinusoidally while a proper trigger is used (Ref. 12) to enable detection at a fixed velocity of the medium.

[18] Figure 1 as drawn is not appropriate for nearly normal incidence. In this case the refracted angle θ_r would turn out to be very small and the refracted beam wave vector $\mathbf{k}_R$ would lie beneath both x' and x'' whereas its components perpendicular to the sample velocity $\boldsymbol{v}$ and to the optical c axis would change sign. The theory developed here remains valid provided $\varphi_R\rightarrow-\varphi_R$ and $\theta_R\rightarrow-\theta_R$ and such a sign change would only affect the term proportional to $\sin\varphi_R$ in Eq. (32).

[19] For a slab of Cu_2O the directions of group and phase velocity inside the slab, respectively parallel to the ray vector $\boldsymbol{s}''$ and k_R'', differ by less than one hundreth of a degree for the typical values of pump intensities and diffraction angles that we examine in Sec. V.

[20] The same expression (3) for the phase shift is obtained for spatial contours either along the ray vector path or along that of the wave vector provided that the end points of the two different contours in the (isotropic) medium outside the slab lie on the same plane orthogonal to the wave vector.

[21] The validity of this expansion relies on the fact that the second and third terms on the right-hand side of Eq. (5) be smaller than n_R^0. For highly dispersive Cu_2O samples the two derivative terms may certainly become quite large, yet for the small sample velocities that we consider in our work the lowest-order refractive index n_R^0 still dominates over the remaining terms on the right-hand side of Eq. (5) so as to keep the expansion valid.

[22] The sign of the effective drag coefficient α_e depends on the specific definition of $\Delta\phi$. Our coefficient α_e in Eq. (9) and α' in Eq. (6) of Ref. 12, e.g., differ by a sign as our and the Sanders-Ezeckiel[12] definitions of $\Delta\phi$ differ by a sign themselves. The sign of the drag coefficient α_e is here, however, irrelevant as a change of sign would only manifest itself in the sign of the interferometer frequency beat, but not the magnitude, by which the drag is typically measured (Refs. 9 and 12).

[23] J. Laub, Ann. Phys. (Leipzig) **25**, 175 (1908). See also W. Parks and J. Dowell, Phys. Rev. A **9**, 565 (1974).

[24] S. Harris, Phys. Today **50**(7), 36 (1997); E. Arimondo, in *Progress in Optics*, edited by E. Wolf (Elsevier Science, New York, 1996), p. 257, and references therein.

[25] G. Alzetta, A. Gozzini, L. Moi, and G. Orriols, Nuovo Cimento Soc. Ital. Fis., B **36**, 5 (1976); E. Arimondo and G. Orriols, Lett. Nuovo Cimento Soc. Ital. Fis. **17**, 333 (1976).

[26] D. Fröhlich, A. Nothe, and K. Reimann, Phys. Rev. Lett. **55**, 1335 (1985): D. Fröhlich, Ch. Neumann, B. Uebbing, and R. Wille, Phys. Status Solidi B **159**, 297 (1990).

[27] F. Bassani and G. Pastori Parravicini, *Electronic States and Optical Transitions in Solids* (Pergamon Press, Oxford, 1975), Chap. 6.

[28] P. Yu and M. Cardona, *Fundamentals of Semiconductors* (Springer, Berlin, 1996), Chap. 6.

[29] L.C. Andreani, in *Confined Electrons and Photons*, edited by E. Burstein and C. Weisbuch (Plenum Press, New York, 1995), p. 57.

[30] In the literature, the Γ_2^+ and Γ_5^+ $1S$ excitons are somewhat inappropriately referred to, respectively, as *paraexciton* and *orthoexciton*.

[31] The Γ_5^- $2P$ states associated to the Γ_2^+ $1S$ state could mix with those associated to the Γ_5^+ $1S$ states, thereby acquiring a spin-singlet component. However, as discussed in the text, we assume that the interactions splitting and mixing the $2P$ manifold are either large compared to Ω_c, in which case we can restrict ourselves to the Γ_4^- dipole active states, or negligible, in which case we do not need to consider the Γ_5^- pure spin triplet.

[32] We only examined one choice of polarization in Ref. 13, and we implicitly assumed a nondegenerate $2P$ manifold.

[33] S. Nikitine, J.B. Grun, and M. Sieskind, J. Phys. Chem. Solids **17**, 292 (1961); in *Semiconductors*, edited by E. O. Madelung, Landolt-Börnstein, New Series Group III, Vol. 17 (Springer, Berlin, 1984).

[34] M. Born and E. Wolf, *Principles of Optics*, 6th ed. (Pergamon Press, Oxford, 1993), Chap. 14.3.

[35] Note that in actual light-drag measurements the laboratory frame polarization of the probe electric field $\boldsymbol{E}$ has to be determined from the one in the slab rest frame S'' in accordance with the transformations (Ref. 15) connecting electric field vectors in the two frames S and S''.

[36] Smaller exciton dephasings would also produce a transparency increase which would clearly favor the light-drag measurement.

[37] In this case, however, Cu_2O would exhibit very low degrees of transparency (Ref. 13).

[38] M. Horne *et al.*, Phys. Rev. A **28**, 1 (1983).

[39] M. Arif *et al.*, Phys. Rev. A **31**, 1203 (1985).